Noisy Image Segmentation: General Approach and Application to Textile Inspection

KHALED ISSA and HIROSHI NAGAHASHI
Imaging Science and Engineering Lab.
Tokyo Institute of Technology
R2-51, 4259 Nagatsuta-cho, Midori-ku,Yokohama
JAPAN

Abstract: A major problem in noisy image processing is the segmentation of its components. Many computer vision tasks analyze regions after segmenting a given image, then minimize the segmentation error to build a good automatic inspection system. In this paper, we propose a novel segmentation scheme for noisy images which consists of a new denoising method and a modified active contour model. The method can be used as a general technique for noisy image segmentation. Moreover, it is applied in the textile inspection field with a comparable level of competence to that of human inspection.

Key–Words: Automated inspection, Fabric defects, Fabric inspection, Vision-based system

1 Introduction

Visual inspection is an important part of quality control in the textile industry where the defects in raw or processed textile materials are identified. The term ”textile defect” covers various types of faults occurring in the yarn and fabric resulted from the precedent stages of the production. Due to the specific nature of textiles, the defects encountered within textile production must be detected and corrected at early stages of the production process. There are currently over 50 categories of defects known to the weaving process alone. Most of these defects appear only in the direction of motion on the loom (the warp direction) or across the width of the fabric (the pick direction) [1]. Most defects are yarn related, such as mispicks, end outs, or broken yarns. Other defects are caused by slubs, or waste, becoming trapped in the fabric structure as it is created. Additional defects are mostly machine related, and manifest themselves in the forms of structural failures (tears or holes) or machine residue (oil spots or dirt). Coupled with the size and speed of the fabric as it passes over the inspection frame, the wide range of defects serve to add complexity to visual inspection and increase the probability of missed defects [1, 2]. On the other hand, 235 types of defects and their possible cases are discussed [3]. These defects may fall into one of the following classes:

1. ***Local point defects***, like holes and loom fly are characterized by a severe tone change over only a few pixels or very few millimeters.

2. ***Medium scale defects***, are characterized by change of texture over a number of millimeters.

3. ***Extended defects***, exhibiting a linear pattern extending over number of centimeters.

Image denoising is to produce a good estimate of the original image from a noisy observation, and is a basic preprocessing stage for image segmantation, especially for the textile image. Segmentation of noisy image is still a challenging problem and its successful solution is investigated either by simple intensity threshlding or by model based deformation of templates. The former implies that the structures are well separated by unique intensity patterns, whereas the latter requires model templates characteristics for the shape class. A wide variety of approaches for image segmentation procedures are documented in the general image processing literature and many successful algorithms have been proposed and developed [4].

Active contour models [5] are appealing to users as they only require a coarse initialization but then converge to a stable and fully reproducible. The basic idea in active contour models or snakes, is to evolve a curve, subject to constraints from a given image, in order to detect objects in that image. The existing active contour models can be broadly classified into three models according to their representation and implementation, i.e., parametric active contour models,

geometric active contour models, and geodesic active contour models.

In this paper, we present a new active contour model that enables to segment the non-uniform noise image efficiently. Segmentation procedure starts with de-noising an image by Log-Gabor filters. Then the image gradient is used to drive an automatic initialization of a level set contour towards the object. Image forces are balanced with global smoothness constraints to converge a smooth object stably. The definition and the use of Log-Gabor filters in the fabric segmentation application are explained in section 2. In section 3, the proposed active contour models is introduced. The model is a combination of the classical image-gradient based active contour and mean curvature moving technique. Finally in section 4, some results are given to prove the effectiveness of the algorithm with respect to noisy image segmentation and fabric defect detection. Conclusions are drawn in section 5.

2 Denoising Scheme

Image denoising is typically done by transforming an image into some domain where the noise component is more easily identified, a threshlding operation is then applied to remove the noise, and finally the transformation is inverted to reconstruct a noise free image. If the noise in the image is not normally distributed or non-uniform, the isotropic smoothing Gaussian will not be effectively used to remove the noise.

Field [6] suggests that natural images are better coded by filters that have Gaussian transfer function when viewed on the logarithmic frequency. The log-Gabor function has Gaussian transfer function when viewed on the logarithmic scale and only can be numerically constructed in the spatial domain via the inverse Fourier transform.

The present log-Gabor wavelet scheme has already been shown efficient in image de-noising [7, 8]. Most currently used de-noising methods are based on anisotropic diffusion [9, 10] or wavelet thresholding [11, 12, 13]. Wavelet or multi resolution image denoising applications usually proceed in three stages, i.e., a transformation, a thresholding and an inverse transform for reconstructing the image.

1. ***Transformation***

   The transform aims at describing the signal of an image in a frequency domain where edges of the image induce high amplitude while spatially incoherent noise produces a low level of amplitude. In the frequency domain the even symmetric filter is represented by two real-valued log-Gaussian projections symmetrically placed on each side of the origin as shown in Fig. 1. The odd-symmetric filter is represented by two imaginary valued log-Gaussian projections anti-symmetrically placed on each side of the origin. One can combine the convolution of the even and odd symmetric filters into one operation. Exploiting the linearity of the Fourier Transform where; $\texttt{FFT}(A + B) = \texttt{FFT}(A) + \texttt{FFT}(B)$, one can do the following: Multiply the FFT of the odd-symmetric filter by i ($i^2 = -1$) and add it to the FFT of the even symmetric filter. The anti-symmetric projections from the odd-symmetric filter will cancel out the corresponding symmetric projection from the even-symmetric filter. This leaves a single projection (multiplied by 2) on the positive side of the frequency spectrum as shown in Fig. 2. Thus if we construct a filter in the frequency domain with a

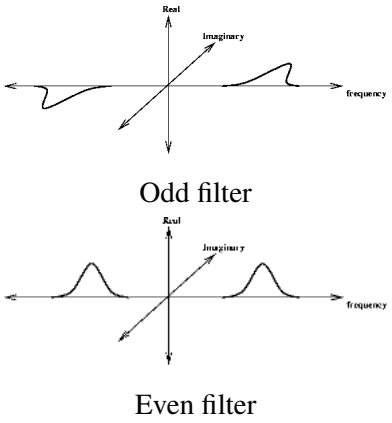

Fig. 1 : Odd and Even symmetric filters transfer functions

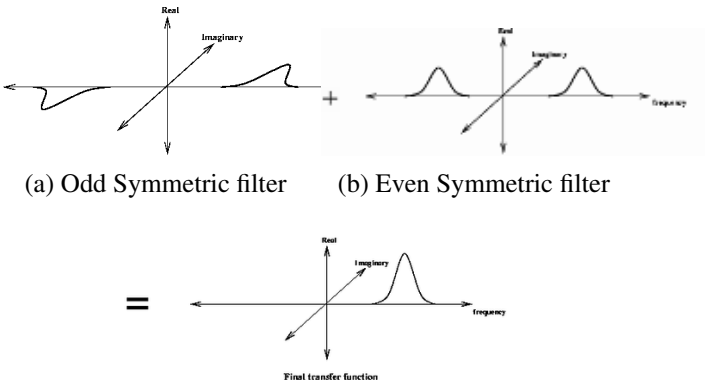

Fig. 2 : Combination of odd and even symmetric filters transfer function

single log-Gabor projection on the positive side of the frequency spectrum, we can consider this filter to be the sum of the FFTs of the even and odd symmetric filters (with the odd symmetric filter multiplied by i). If we perform the convolution by multiplying this frequency domain filter by the FFT of the image and take the inverse FFT we end up with the even-symmetric convolution residing in the real part of the result and the odd-symmetric convolution residing in the imaginary part.

Let $\boldsymbol{M}_{so}^{even}$ and $\boldsymbol{M}_{so}^{odd}$ denote the even-symmetric and odd-symmetric filters at scale *s* and orientation *o*, respectively. So the response vector can be calculated by:

$$[\boldsymbol{E}_{so}(x,y), \boldsymbol{O}_{so}(x,y)] = [\boldsymbol{I}(x,y) * \boldsymbol{M}_{so}^{even}, \boldsymbol{I}(x,y) * \boldsymbol{M}_{so}^{odd}] \quad (1)$$

The amplitude of the response is given by:

$$\boldsymbol{A}_{so} = \sqrt{\boldsymbol{E}_{so}(x,y)^2 + \boldsymbol{O}_{so}(x,y)^2} \quad (2)$$

The phase angle is:

$$\boldsymbol{\theta}_{so}(x,y) = \tan^{-1}\left(\frac{\boldsymbol{O}_{so}(x,y)}{\boldsymbol{E}_{so}(x,y)}\right) \quad (3)$$

A more sensitive phase deviation measure can be calculated by :

$$\triangle\boldsymbol{\theta_{so}}(\boldsymbol{x},\boldsymbol{y}) = \cos(\boldsymbol{\theta}_{so}(x,y) - \bar{\boldsymbol{\theta}}_0(x,y)) - \sin(\boldsymbol{\theta}_{so}(x,y) - \bar{\boldsymbol{\theta}}_0(x,y)) \quad (4)$$

Where $\triangle\boldsymbol{\theta}_{so}(x,y)$ is the mean phase angle at orientation (o). Six orientations and six scales are used in this research.

2. ***Thresholding***

The basic thresholding technique permits to segregate most of the signal from the noise. There exists many methods for determining the optimal threshold [11, 12, 16]. Additionally, more elaborated methods that take into account the neighborhood of each coefficient have been introduced [12, 13]. In this research the noise is taken to be:

$$\boldsymbol{T} = \boldsymbol{\mu}_r + k\boldsymbol{\sigma}_r \quad (5)$$

where, μ_r is the mean noise response, σ_r is the standard deviation, and *k* is a constant range from 2 to 3. According to Kovesi [14], the magnitude of the response vector to a pure noise signal will form like Rayleigh distribution.

$$\boldsymbol{R}(x) = \frac{x}{\sigma_g^2} exp^{\frac{-x^2}{2\sigma_g^2}}, \quad (6)$$

where σ_g^2 is the variance of 2D normal distribution describing the position of total energy vector. The mean and variance of the Rayleigh distribution are given by :

$$\boldsymbol{\mu}_r = \sigma_g\sqrt{\frac{\pi}{2}} \quad (7)$$

$$\boldsymbol{\sigma}_r^2 = \frac{4-\pi}{2}\sigma_g^2 \quad (8)$$

Taking into consideration that the smallest scale filter has the largest bandwidth and will give the strongest noise response [14], the smallest scale wavelet quadrature pair will spend most of their time only responding to noise. A robust estimation of the mean amplitude response of the smallest scale filter can be obtained via the value of the median of the Rayleigh distribution *x* such that:

$$\int_0^x \frac{x}{\sigma_g^2} exp^{\frac{-x^2}{2\sigma_g^2}} = \frac{1}{2} \Rightarrow Median = \sigma_g\sqrt{-2\ln(1/2)} \quad (9)$$

Accordingly, the mean and standard deviation can be estimated and the noise amplitude distribution can be determined.

3. ***Back Transformation***

In this step, a reverse transform is applied for reconstructing the image. Fig. 3 shows the denoising processing of an image using logGabor filter, and one example of the process for a synthetic image is illustrated in Fig. 4.

3 Modified Active Contour Model

Refereing to Fig. 4, it can be seen that the Log-Gabor filter did not completely remove the noise from the image and some noisy spikes still exist. A level set approach can remove the remaining spikes and segment the image. The idea is to view the pixel values as a topographic map; the intensity (somewhere between white and black) at each pixel is the height of the surface at that point. In a deformable model segmentation scheme, the model is driven by image forces and

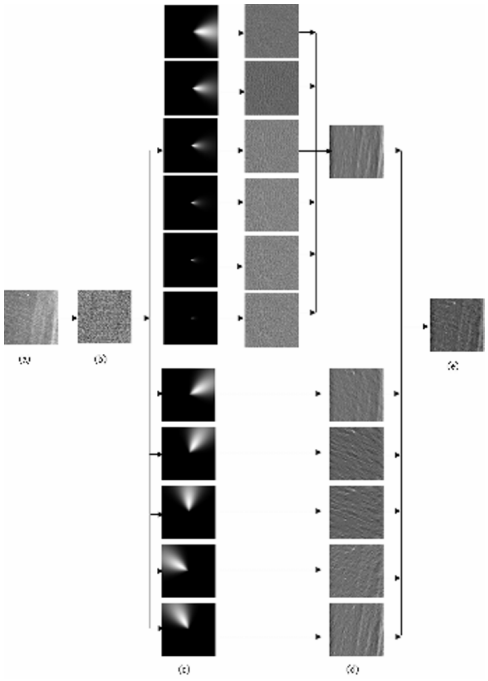

Fig. 3 : Image processing using logGabor filter

(a) Original image, (b) Amplitude spectrum, (c) Fourier domain logGabor filter, (d) Filter response with different orientations and scales, (e) Filtered image
(The upper images in the third column shows the filter response with different scales)

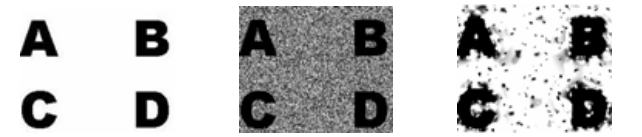

(a) Original image (b)Noisy image (c)Smoothed image

Fig. 4 : Noise removal using Log-Gabor filter

constrained by prior information on the shape of the model. In a classical active contour, the image forces are governed by the gradient magnitude and the shape prior is a form of smoothness. Meanwhile, in the Chan and Vese model [15], the contour is evolved by the mean curvature flow.

The proposed active contour model is a combination of the classical active contour based on the image gradient and the mean curvature moving technique. Consider the evolution of the set function C such that its zero set tracks the evolving contour at a constant speed v. We use the image gradient for moving the contour given by,

$$\frac{\partial C}{\partial t} = v \cdot e(|\nabla \boldsymbol{I}|) \tag{10}$$

where, $e(|\nabla \boldsymbol{I}|)$ is a decreasing edge function given by $e(|\nabla \boldsymbol{I}|) = c^2/(c^2 + |\nabla \boldsymbol{I}|^2)$ and controlled by a free parameter c that determines the constant of edges, and v is the speed of contour movement. The initial set function C_0 is given by the following equation:

$$C_0 = \begin{cases} -\epsilon, & (x,y) \in \Omega_0 - \partial\Omega_0 \\ 0 & (x,y) \in \partial\Omega_0 \\ \epsilon & \Omega - \Omega_0 \end{cases} \tag{11}$$

Where: Ω_0 is a subset in the image domain Ω, and $\partial\Omega_0$ denotes all the points on the boundaries of Ω_0. There are two kinds of energies which drive the contour towards the objects. Outside force $\boldsymbol{F}_o$ that pushes the contour towards the object and internal force $\boldsymbol{F}_{in}$ and these forces are related as follows,

$$\frac{\partial C}{\partial t} = v(\boldsymbol{F}_{in} - \boldsymbol{F}_o) \cdot e(|\nabla \boldsymbol{I}|) \tag{12}$$

The term $\boldsymbol{F}_{in} - \boldsymbol{F}_o$ represents the image forces that used to drive the contour towards the object, so that the contour may shrink when it encloses parts of the background and may grow when the contour is inside the object.

The image forces need to be balanced with some smoothness constraints; a standard technique is to apply the mean curvature flow to the contour that is the length of the contour and the area inside it. The strength of the smoothing is controlled with the constant factors μ_1 and μ_2.

$$\begin{aligned} \frac{\partial C}{\partial t} &= v\left[(\boldsymbol{F}_{in} - \boldsymbol{F}_o) \cdot e(|\nabla \boldsymbol{I}|)\right. \\ &\quad + \mu_1 \left(\triangle C - div(\frac{\nabla C}{|\nabla C|}) \cdot e(|\nabla \boldsymbol{I}|)\right) \\ &\quad \left. - \mu_2 |\nabla \boldsymbol{C}|\right. \end{aligned} \tag{13}$$

where $\triangle$ is the Laplacian operator. Lastly, smoothness constraints are applied to the contour in order to prevent it from leaking into small noise structures in the image that is not part of the target objects. The smoothing behavior is defined by the relationship between the derivative magnitude in the gradient direction and the derivative in the direction of level set. The strength of the smoothness is controlled by constant factor ν as shown in Eq.(14). This additional constraints is used to control whether the curvature flow is applied or not, and thus to stop the curvature motion once the smallest spikes are removed. This will make the very small contours disappear which correspond to spikes of noise, however the boundaries will remain sharp, since they will not blur under this

Table 1 : Results of fabric defect detection

	Defects type		
	Local defects	Medium defects	Extended defects
Overall detection rate	94/100	91/100	87/100

motion, and instead only move according to their curvature as illustrated in Fig. 5.

In the next examples (illustrated in Fig. 6 and Fig. 7), we discuss the comparisons between the original active contour eq.(12) and the proposed active contour for detecting objects without gradient and detecting multi-objects in noisy images.

$$\frac{\partial C}{\partial t} = v[(\boldsymbol{u}F_{in} - \boldsymbol{u}F_o) \cdot e(|\nabla \boldsymbol{u}I|) + \mu_1 \left(\triangle C - div(\frac{\nabla C}{|\nabla C|}) \cdot e(|\nabla \boldsymbol{u}I|) \right) - \mu_2 |\nabla \boldsymbol{u}C| + \nu \cdot div(\frac{\nabla C}{|\nabla C|})] \quad (14)$$

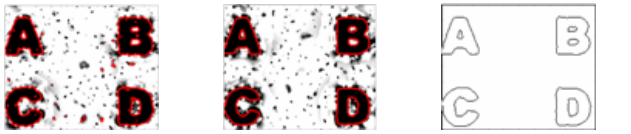

(a)Initiative contours (b)Final contour (c)Binariezed image

Fig. 5 : Image segmentation using active contour

4 Experimental Results and Discussion

The proposed approach has been tested using the TILDA database [17], realized by the Technische Universitat Hamburg in 1996, which consists of 8 different textiles materials without known orientation. Examples of results obtained are shown in Fig. 8, and the experimental results are summarized in Table 1. The method is more flexible for the detection of single and multiple defects in woven and knitted fabrics for both single and extended defects.

5 Conclusion

A novel segmentation scheme for noisy image was presented in this paper, which consisits of a new denoising method and modified active contour model.

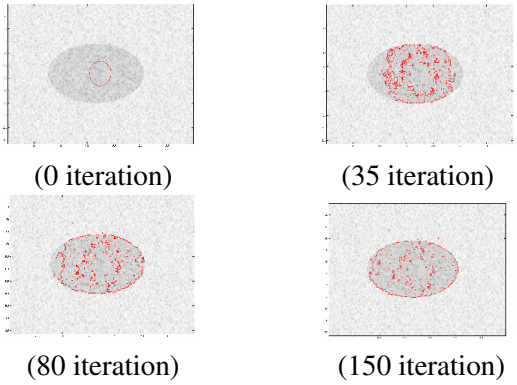

(0 iteration) (35 iteration) (80 iteration) (150 iteration)

(a) Original active contour

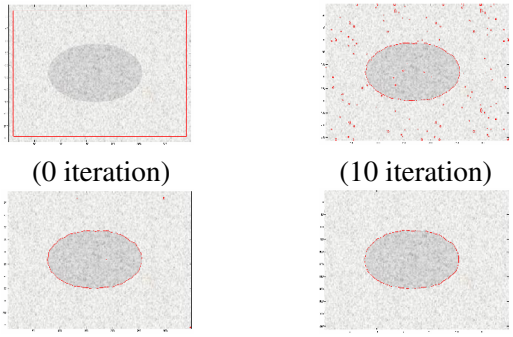

(0 iteration) (10 iteration) (25 iteration) (30 iteration)

(b) Modified active contour

Fig. 6 : Detection of object without gradient

This method was tested for natural and synthetic images and showed promising results.

References:

[1] H. Sari-Sarraf and J.Jr. Goddard, Vision system for on-loom fabric inspection, *IEEE Transactions on Industry Applications*, Vol.36, No.6, 1999, pp.1252-1259.

[2] A. Baykut, A. Atalay, A. Ercil, and M. Guler, Real-time defect inspection of textured surfaces, *Real-time Imaging*, Vol.6, 2000, pp.17-27.

[3] K. Srinivasan, P.H Dastor, P. Radhakrishnaihan, and S. Jayaraman, A knowledge-based frame-detection work for analysis of defects in wovwn textile structure, *J.Text.Inst.* Vol.83, 1992, pp.431-447.

[4] K.S.Fu and J.K.Mui, A survey of image segmentation, *Pattern Recognation*, Vol.13, No.1 1981, pp.3-16.

[5] M.Kass, A.Witkin, and D. Terzopoulos, Snakes: active contour models, *Int.J.Comp.Vis*, Vol.1, 1988, pp.321-331.

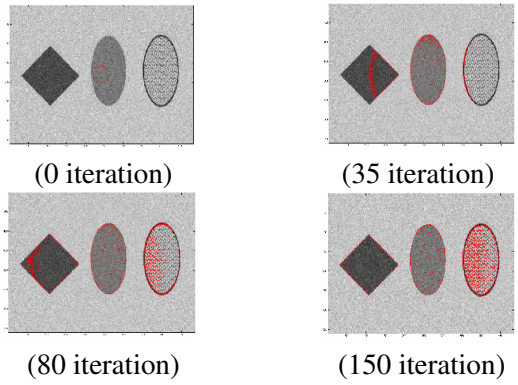

(a) Original active contour

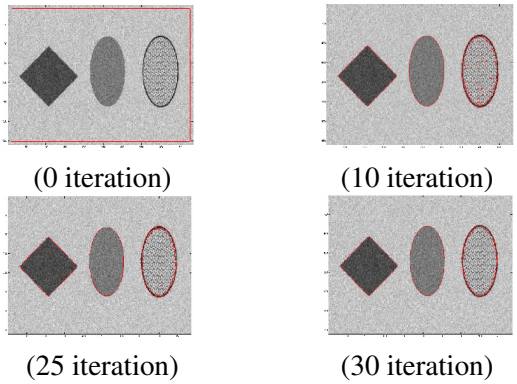

(b) Modified active contour

Fig. 7 : Detection of different objects from a very noisy image

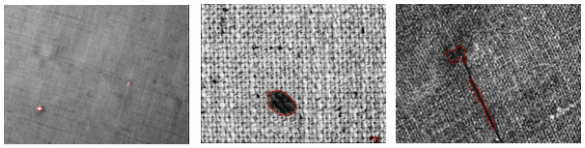

(a) local defect

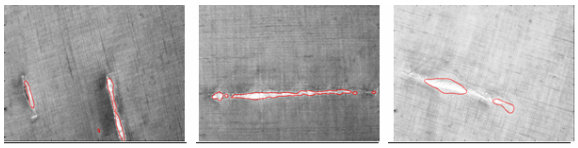

(b) medium defect

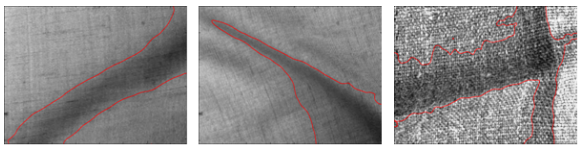

(c)extended defect

Fig. 8 : Results of processing fabric images

[6] D.J. Field, Relation between the statistics of natural images and the response properties of cortical cells, *Journal of the Optical Society of America*, Vol.A4, No.12, 1987, pp.2379-2394.

[7] S.Fischer, R.Redondo, L.Perrinet, and G.Cristobal, Spars gabor wavlets by local operations, *Proc.SPIE Bioengineered and Bioinspired Systems*, Vol.II, No.5839, 2005, pp.75-86.

[8] R. Redondo, S. Fischer, L. Perrinet, and G. Cristobal, Modeling of simple cells through a sparse overcomplete gabor wavelet representation based on local inhibition and facilitation, *European Conf. On Visual Perception*, 2005.

[9] F. Sroubek and J. Flusser, Multichannel blind iterative image restoration,*IEEE Trans. Image Proc.*, Vol.12, No.9, 2003, pp.1094-1106.

[10] A. B. Hamza, H. Krim, and G. Unal, Unifying probabilistic and variational estimation, *IEEE Signal Proc.*, Vol.19, No.5, 2002, pp.3747.

[11] D. Donoho, De-noising by soft-thresholding, *IEEE Trans. Inf. Theory*, Vol.41, No.3, 1995, pp.613-627.

[12] S. G. Chang, B. Yu, and M. Vetterli, Adaptive wavelet thresholding for image denoising and compression, *IEEE Trans. on Image Proc.*, Vol.9, No.9, 2000, pp.1532-1546.

[13] J. Portilla, V. Strela, M. Wainwright, and E. Simoncelli, Image denoising using scale mixtures of gaussians in the wavelet domain, *IEEE Trans. Image Proc.*, Vol.12, No.11, 2003, pp.1338-1351.

[14] Kovesi, Image features from phase congruency, *Journal of Computer Vision Research*, Vol.1, No.3, 1999, pp.1-26.

[15] T. Chan and L. Vese, Active contours without edges, *IEEE Trans. Image. Proc.*, Vol.10, 2001, pp.266-277.

[16] C. Taswell, The what, how and why of wavelet shrinkage denoising, *Computing in Science and Engineering*, 2000, pp.12-19.

[17] Technische Universitt Hamburg-Harburg ,*Ein referenzdatensatz zur evaluierung von sichtprfungsverfahren fr textiloberflchen*, Interner bericht 96, 1996.